ChemComm

COMMUNICATION

View Article Online
View Journal

Cite this: DOI: 10.1039/d2cc06381f

Received 24th November 2022,
Accepted 30th November 2022

DOI: 10.1039/d2cc06381f

rsc.li/chemcomm

Experimental observation of metal–organic framework–polymer interaction forces and intercalation†

Joseph M. Palomba, ‡[a] Verda Saygin ‡[b] and Keith A. Brown *[bc]

We attach a MOF crystallite to an atomic force microscope cantilever to realize a system for rapidly and quantitatively studying the interaction between single-crystal MOFs and polymer films. Using this method, we find evidence of polymer intercalation into MOF pores. This approach can accelerate composite design.

Metal–organic frameworks (MOFs) are crystalline porous solids constructed from inorganic nodes and organic ligand struts. These materials have gained tremendous attention over the past three decades for their record-breaking internal surface areas, chemical tunability, and achievements in molecular sorption for gas storage and separation.[1–4] Despite their promise, the translational impact of MOFs has been slowed because their limited processability and stability compared to other porous materials such as activated carbon or zeolites. MOFs have been introduced to polymer–matrix composites to address these challenges, but fundamental gaps remain in understanding the polymer–MOF interface.[5–7] Further, such research is often motivated by gas permeation applications[8,9] and thus characterization has largely focused on small molecule gas separations with efforts focusing on realizing ''ideal'' interfaces rather than predictive design.[8,10–14]

Recent work has sought to elucidate the MOF–polymer interface through indirect or qualitative means. For example, electron microscopy studies have explored the distributions of MOF particles in a polymer matrix.[15] Ensemble measurements, such as 2D nuclear magnetic resonance (NMR) spectroscopy, have explored polymer infiltration into MOFs to study the chemical differences that affect sorption.[16–18] Molecular dynamics (MD) simulations have been used to identify features important to MOF–polymer composite performance.[10,17,19–21] Such studies have yet to be paired with direct experiential measurement of MOF–polymer interactions.

When considering quantitative interface science, atomic force microscopy (AFM) stands out as a workhorse tool. In addition to creating high-resolution topographic maps of surfaces, AFM can also perform precise nanoindentation experiments to quantify pico- to micro-Newton forces and therefore evaluate mechanical properties such as Young's modulus, hardness, and adhesion.[22–24] The question then, is how could one use a silicon AFM probe to measure the interaction between a MOF and a polymer? Interestingly, researchers have functionalized AFM probes with molecules, polymers, peptides, *etc.* to study the interaction between materials with molecular precision[25] or even replaced the tip of the probe entirely with a sphere to simplify nanomechanical analysis.[24,26] In one relevant case, oligomers were attached to AFM tips to study their interaction with MOFs as a comparison to MD simulations of oligomer diffusion.[16] These studies found qualitative agreement but specific interactions could not be derived from these experiments.

In this study, a novel method is presented for quantitatively probing MOF–polymer interfaces using a MOF particle attached to a tipless AFM cantilever (Fig. 1). By controllably adding a picoliter of epoxy to a tipless AFM cantilever, a single MOF particle can be affixed to the cantilever creating a precise, facet–specific nanoindenter. Comparing a MOF-tipped probe interacting with a polymer film and a polymer-tipped probe interacting with a MOF, we note three key advantages inherent to the MOF-tipped probe. (1) Changing the sample does not influence the AFM calibration, so adhesion forces measured for a MOF-tipped probe on different polymers can be compared without recalibration. (2) Performing a nanoindentation experiment on a MOF crystallite involves the extra step of finding the MOF crystallite and aligning the probe tip with the crystallite. (3) Using a MOF-tipped probe allows the contact area, any defects, and crystal orientation to be defined consistently, which both facilitates quantitative comparison and

[a] *Soldier Protection Directorate, U.S. Army Combat Capabilities Development Command Soldier Center, Natick, MA, 01760, USA*
[b] *Department of Mechanical Engineering, Boston University, 110 Cummington Mall, Boston, Massachusetts 02215, USA. E-mail: brownka@bu.edu*
[c] *Physics Department and Division of Materials Science and Engineering, Boston University, 590 Commonwealth Avenue, Boston, Massachusetts 02215, USA*

† Electronic supplementary information (ESI) available. See DOI: https://doi.org/10.1039/d2cc06381f

‡ These authors contributed equally to this work.

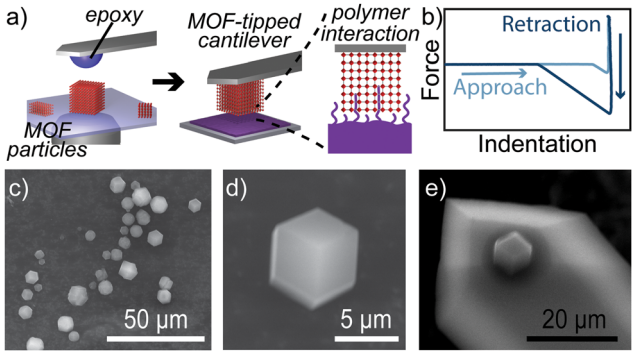

Fig. 1 (a) Schematic showing the preparation of a MOF-tipped cantilever and possible polymer interaction between the tip and polymer surface during nanoindentation. (b) Schematic of force–indentation curve showing the probe approach and retraction curves. (c and d) Scanning electron microscope (SEM) images of synthesized ZIF-8 MOF crystals. (e) SEM image of prepared MOF-tipped AFM cantilever.

enables control over the facet of interest. To study the implications of this tool for analyzing MOF–polymer interfaces, a set of eight surfaces were analyzed with the MOF-tipped probe and compared to measurements taken using a probe with a similarly-sized non-porous silica bead tip. These experiments showed that MOF-tipped probes can obtain adhesion forces that are reflective of properties of the interface, namely work of adhesion. However, we also observe anomalously high adhesion when studying polyisobutylene (PIB), which we attribute to polymer chains intercalating into the pores of the MOF, providing an example of how this approach can shine light on important questions regarding MOF–polymer interactions. Given the vast number of MOF compositions, processing conditions, and environmental factors that can potentially impact the MOF–polymer interface, high throughput methods for assessing these factors is of high value.

Zeolitic imidazolate framework-8 (ZIF-8) was chosen as the MOF for this study as it is stable in ambient conditions and readily grown as micron-size crystals.[27,28] To prepare the MOF-tipped cantilever, the ZIF-8 crystals (Fig. S1 and S2, ESI†) were deposited on a glass slide next to a reservoir of two-part epoxy. A tipless cantilever with $\sim$40 N m^{-1} stiffness was then dipped into a small reservoir of two-part epoxy to retrieve a picoliter-scale droplet of epoxy, following our reported methods of fluid handling.[29] The cantilever with epoxy was then brought into contact with an isolated MOF particle, allowing the MOF to be picked up and attached to the end of the cantilever (Fig. 1a). After the cantilever was cured for 24 hours, it was imaged using scanning electron microscopy (SEM) to validate the attachment process. In a successful process, a single MOF crystal was observed at the end of the cantilever (Fig. 1e). The ZIF-8 crystal had a rhombic dodecahedral crystal habit that exposes the (110) plane on all faces. Importantly, this means that the exposed chemical groups and pores are known. Recent synthetic advances show that it is possible to control the crystal habit and therefore the exposed planes.[30] Thus, it is possible to examine facet–specific interactions. While measurements are in principle possible with any size MOF, the range of MOF crystals that can be practically attached to a cantilever is expected to be $\sim$1–45 μm. As many MOFs are formed as nanocrystals, future work will focus on sub-micron particles.

We hypothesized that MOF-tipped probes could perform meaningful nanoindentation experiments, a non-obvious hypothesis given how different in shape and structure these are from conventional AFM probes. To test this, a series of nanoindentation experiments were conducted on fluorosilane-coated, untreated, and plasma-cleaned silicon surfaces as model flat surfaces that vary in their surface energy (Fig. S3, ESI†). Nanoindentation experiments were conducted on each surface by measuring 36 force–indentation curves in a 50 $\times$ 50 μm^2 grid with the $\sim$9 μm MOF indenter. A minimum of 108 distinct indentation curves were taken for each condition. Force–indentation curves for these surfaces all show a flat approach, single contact point, and subsequent linear increase, all consistent with standard nanoindentation curves. Further, the adhesion force, *i.e.* the largest negative force recorded during each force–indentation curve, was reproducible (Fig. S4, ESI†) and increased in magnitude with surface hydrophilicity, as expected. After these experiments, the MOF-tipped cantilever was reimaged with SEM and no visible degradation was observed (Fig. S5, ESI†). These results show that the MOF-tipped probe functions reliably and repeatedly as an AFM tip.

With confidence in the MOF-tipped probe as a nanoindentor, a series of four polymers were used for a MOF–polymer interface investigation. The polymers chosen for this study were polyvinylidene difluoride (PVDF), polyethylene oxide (PEO), polystyrene-*block*-polybutadiene-*block*-polystyrene (SBS), and PIB for their range of physical properties and chemical structure. At room temperature, PVDF is a semi-crystalline hydrophobic polymer while PEO is a semi-crystalline hydrophilic polymer. In contrast, SBS and PIB are both hydrophobic polymers in their rubbery state at room temperature, but differ in the width of the polymer chains. Notably, PVDF, PEO, and SBS have all been studied as matrices for MOF composites.[20] Interestingly, MD simulations and 2D NMR have shown that high molecular weight (900 kg mol^{-1}) dissolved PEO can intercalate into a zirconium MOF (UiO-66).[17] Confident that these polymers would provide a diverse array of polymer properties, substrates were prepared on silicon surfaces by spin-coating dilute polymer solutions. Film thickness was measured using variable angle spectroscopic ellipsometry and film roughness was measured using conventional AFM (Fig. S6, ESI†). The roughness of all films was $<$7 nm (Table S3, ESI†). As this is substantially smaller than the contact diameter, it is not expected to strongly influence the contact force.

To study the properties of the MOF–polymer interfaces, nanoindentation experiments were conducted on each polymer sample using the same protocol as described for the silicon surfaces (Fig. S7, ESI†). All indentation curves showed a single contact point and repeatable adhesion force (Fig. S8, ESI†). Examining the range of the interactions, however, the interaction of the MOF-tip with PIB was significantly longer range than all the others, highlighting that further effects may be at play beyond simple rigid contact.

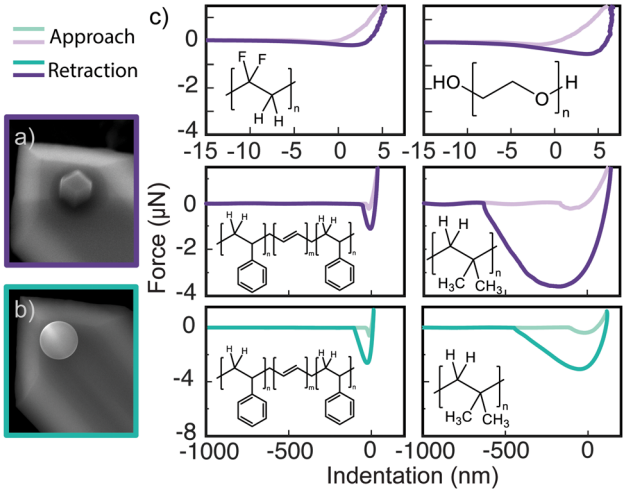

Fig. 2 SEM images of MOF-tipped (a) and bead-tipped (b) AFM cantilevers and force–indentation curves on polymer surfaces (c) PVDF, PEO, SBS, and PIB taken using MOF-tipped probe (purple) and SBS and PIB taken using bead-tipped probe (teal).

To interpret these results, nanoindentation measurements were repeated with a solid spherical nanoindentor as a control. In particular, a tapping mode cantilever with a ~10 μm diameter spherical silica bead tip was selected to have the same cantilever stiffness as the MOF-tipped probe and a commensurate contact area during nanoindentation (Fig. 2b). Identical nanoindentation experiments were repeated on all the polymer films with the bead-tipped probe. The shape of the indentation curves for bead-tipped probe on PVDF, PEO, and SBS resembled those of the MOF-tipped probe (Fig. 2c and Fig. S6, ESI†). Interestingly, the bead-PIB indentation curve had the highest adhesion and range of the polymer surfaces tested (Fig. 2c), but both metrics were still lower than those measured using the MOF-tipped probe.

In addition to studying polymer composition, this method can explore the role of other structural or processing details. For instance, we tested whether polymer film thickness affected pull-off force by preparing a second SBS film that was 144 nm thick (SBS-B), which was thinner than the 873 nm thick film studied previously (SBS-A). Interestingly, the MOF had an ~38% higher average pull-off force on the thin film relative to the thick film. This increase matched the increase observed between the bead and these films. We note that a transition from elastic to rigid contact is theoretically accompanied by a 33% increase in pull-off force.[31] To explain why such a change in contact behavior would occur for the same material, we note that thin soft films on rigid surfaces exhibit vastly increased stiffness due to the substrate effect and this effect is more pronounced for larger indenters.[24]

To better understand these nanoindentation experiments, the adhesion force for both probes were plotted (Fig. 3a). For adhesion forces based solely on classical solid–solid contact, one would expect adhesion force for each system to be proportional to the work of adhesion times a geometric factor. Thus, the ratio of the force measured by one probe and another of similar material would be expected to be consistent. Evaluating the data, it is clear that the adhesion forces for PVDF, PEO, and both SBS samples were well-fit by a line through the origin, suggesting that for these materials, the bead and MOF were interacting with the surface through classical solid–solid contact with the ratio of the force illustrating the ratio of the effective probe sizes (Fig. 3a). While this was an excellent fit (R^2 = 0.9967), the PIB data point was substantially more than five standard deviations from the line, indicating that the MOF–PIB interaction was not classic solid–solid contact.

To explain the observed anomalously high force and range of the MOF–PIB interaction, we hypothesized that PIB chains were intercalating into the pores of the ZIF-8 crystal upon contact (Fig. 3b and c). PIB chain intercalation in the pores of MOF explains not only the increased adhesion force, but also the ~1 μm range, which is commensurate with the PIB chain length.[32] As the cantilever was retracted, we hypothesize that the polymer chains continued to exert force on the MOF, resulting in an attraction between the MOF and sample. This effect of polymer chain intercalation into MOF pores has been observed for semi-crystalline polymers in solution,[17] but never for a MOF–polymer interface in air. By using a rubbery polymer with high chain mobility at room temperature, this is the first experimental observation of polymers intercalating into MOF pores outside solution. Despite the small (3.4 Å) crystallographic pore size of ZIF-8, framework flexibility has accounted for sorption of larger molecules such as isobutylene (4.8 Å). PIB intercalation is further supported by the lack of intercalation observed for SBS, whose larger monomer diameter (~6.6 Å)[33] prevents it from fitting within the pores.

One implication of these results is that PEO does not intercalate within this MOF, which might seem to contradict prior reports of PEO inside the pores of related MOFs. That said, all prior observations of PEO intercalation either do so in solution or at an elevated temperature at which PEO would be melted.[34] Here, PEO is semi-crystalline and we hypothesize that it lacks the mobility to enter the pores. This result highlights

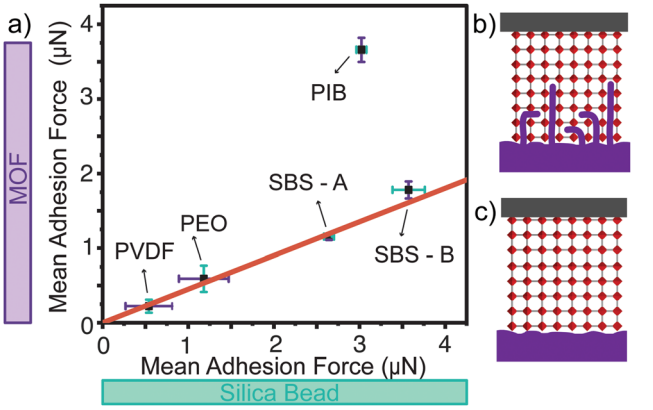

Fig. 3 Mean adhesion forces between both probes and five polymer surfaces with a best fit line (a), and scheme showing polymer infiltration proposed for PIB-MOF (b) *vs.* SBS-MOF (c). (SBS-A thickness 144 nm and SBS-B thickness 873 nm.)

the subtlety that intercalation requires both that the polymer can fit within the pores and that it is mobile enough to do so.

This work presents and validates a new tool for directly characterizing the facet–specific interfaces between MOFs and polymers. As an initial demonstration of the ability of this method to provide insight into the MOF–polymer interface, we report quantitative data on interfacial forces between a MOF and four different polymers that collectively show that PEO does not intercalate in ambient non-solvated conditions and find evidence that PIB does intercalate under ambient conditions. Further, this method is scalable to high-throughput evaluation of many interfaces and thus enables the exploration of a wide chemical and processing space. The goal of future work is use this and other complementary methods to build detailed models of MOF–polymer interfaces that take into account a number of parallel physical and chemical phenomena. For example, one would expect that increasing the polymer molecular weight would lead to fewer chain ends that are available to diffuse into the MOF, thus lowering the additional adhesive force. Similarly, adjusting the end groups of the polymer would be expected to strongly influence intercalation. These and other hypotheses could be explored using this method. Further, AFM is routinely used in liquid environments and at variable temperatures,[35] so the probes described herein could be used to study polymer melts or conditions relevant to biology or energy applications. What makes an ideal MOF–polymer interface for a given application remains an open question, but this work provides a new method for experimentally addressing this question.

J. M. P. and V. S. contributed to investigation, validation, and formal analysis. J. M. P., V. S., and K. A. B. contributed to conceptualization, methodology, visualization, writing – original draft, and writing – review & editing. J. M. P. and K. A. B. contributed to funding acquisition and project administration. J. M. P. and V. S. contributed equally to work and this is reflected in co-primary authorship.

J. M. P. acknowledges the Department of Defense Science, Mathematics, and Research for Transformation (SMART) Program Office, Office of the Undersecretary of Defense for Research and Engineering (OUSDR&E) SEED Grant for funding. V. S. and K. A. B. acknowledge support from the Defense Threat Reduction Agency (HDTRA12210036) and the National Science Foundation (CMMI-1661412). The authors would like to acknowledge Dr Joshua Uzarski for helpful discussions.

Conflicts of interest

There are no conflicts to declare.

Notes and references

1 H. Furukawa, K. E. Cordova, M. O'Keeffe and O. M. Yaghi, *Science*, 2013, **341**, 1230444.
2 A. Kirchon, L. Feng, H. F. Drake, E. A. Joseph and H.-C. Zhou, *Chem. Soc. Rev.*, 2018, **47**, 8611–8638.
3 D. S. Sholl and R. P. Lively, *Nature*, 2016, **532**, 435–437.
4 B. M. Weckhuysen and J. Yu, *Chem. Soc. Rev.*, 2015, **44**, 7022–7024.
5 M. Kalaj, K. C. Bentz, S. Ayala, J. M. Palomba, K. S. Barcus, Y. Katayama and S. M. Cohen, *Chem. Rev.*, 2020, **120**, 8267–8302.
6 J.-O. Kim, J. Y. Kim, J.-C. Lee, S. Park, H. R. Moon and D.-P. Kim, *ACS Appl. Mater. Interfaces*, 2019, **11**, 4385–4392.
7 G. W. Peterson, M. A. Browe, E. M. Durke and T. H. Epps, *ACS Appl. Mater. Interfaces*, 2018, **10**, 43080–43087.
8 T.-S. Chung, L. Y. Jiang, Y. Li and S. Kulprathipanja, *Prog. Polym. Sci.*, 2007, **32**, 483–507.
9 J. Winarta, A. Meshram, F. Zhu, R. Li, H. Jafar, K. Parmar, J. Liu and B. Mu, *J. Polym. Sci.*, 2020, **58**, 2518–2546.
10 I.-D. Carja, S. R. Tavares, O. Shekhah, A. Ozcan, R. Semino, V. S. Kale, M. Eddaoudi and G. Maurin, *ACS Appl. Mater. Interfaces*, 2021, **13**, 29041–29047.
11 S. R. Venna, M. Lartey, T. Li, A. Spore, S. Kumar, H. B. Nulwala, D. R. Luebke, N. L. Rosi and E. Albenze, *J. Mater. Chem. A*, 2015, **3**, 5014–5022.
12 Z. Wang, H. Ren, S. Zhang, F. Zhang and J. Jin, *J. Mater. Chem. A*, 2017, **5**, 10968–10977.
13 G. W. Peterson, H. Wang, K. Au and T. H. Epps III, *Polym. Int.*, 2021, **70**, 783–789.
14 R. Thür, N. Van Velthoven, V. Lemmens, M. Bastin, S. Smolders, D. De Vos and I. F. J. Vankelecom, *ACS Appl. Mater. Interfaces*, 2019, **11**, 44792–44801.
15 T. Rodenas, M. van Dalen, E. García-Pérez, P. Serra-Crespo, B. Zornoza, F. Kapteijn and J. Gascon, *Adv. Funct. Mater.*, 2014, **24**, 249–256.
16 T. Uemura, G. Washino, S. Kitagawa, H. Takahashi, A. Yoshida, K. Takeyasu, M. Takayanagi and M. Nagaoka, *J. Phys. Chem. C*, 2015, **119**, 21504–21514.
17 P. Duan, J. C. Moreton, S. R. Tavares, R. Semino, G. Maurin, S. M. Cohen and K. Schmidt-Rohr, *J. Am. Chem. Soc.*, 2019, **141**, 7589–7595.
18 N. Oe, N. Hosono and T. Uemura, *Chem. Sci.*, 2021, **12**, 12576–12586.
19 R. Semino, N. A. Ramsahye, A. Ghoufi and G. Maurin, *ACS Appl. Mater. Interfaces*, 2016, **8**, 809–819.
20 R. Semino, J. C. Moreton, N. A. Ramsahye, S. M. Cohen and G. Maurin, *Chem. Sci.*, 2018, **9**, 315–324.
21 S. M. Vornholt, M. J. Duncan, S. J. Warrender, R. Semino, N. A. Ramsahye, G. Maurin, M. W. Smith, J.-C. Tan, D. N. Miller and R. E. Morris, *ACS Appl. Mater. Interfaces*, 2020, **12**, 58263–58276.
22 F. L. Leite, C. C. Bueno, A. L. Da Róz, E. C. Ziemath and O. N. Oliveira, *Int. J. Mol. Sci.*, 2012, **13**, 12773–12856.
23 E. Barthel, *J. Phys. D: Appl. Phys.*, 2008, **41**, 163001.
24 L. Li, N. Alsharif and K. A. Brown, *J. Phys. Chem. B*, 2018, **122**, 10767–10773.
25 T. Hugel and M. Seitz, *Macromol. Rapid Commun.*, 2001, **22**, 989–1016.
26 M. Kopycinska-Müller, R. H. Geiss and D. C. Hurley, *Ultramicroscopy*, 2006, **106**, 466–474.
27 B. Chen, Z. Yang, Y. Zhu and Y. Xia, *J. Mater. Chem. A*, 2014, **2**, 16811–16831.
28 D. Saliba, M. Ammar, M. Rammal, M. Al-Ghoul and M. Hmadeh, *J. Am. Chem. Soc.*, 2018, **140**, 1812–1823.
29 V. Saygin, B. Xu, S. B. Andersson and K. A. Brown, *ACS Appl. Mater. Interfaces*, 2021, **13**, 14710–14717.
30 X.-Y. Liu, W.-S. Lo, C. Wu, B. P. Williams, L. Luo, Y. Li, L.-Y. Chou, Y. Lee and C.-K. Tsung, *Nano Lett.*, 2020, **20**, 1774–1780.
31 K. L. Johnson and J. A. Greenwood, in *Encyclopedia of Tribology*, ed. Q. J. Wang and Y.-W. Chung, Springer US, Boston, MA, 2013, pp. 42–49.
32 L. Xia, C. Li, X. Zhang, J. Wang, H. Wu and S. Guo, *Polymer*, 2018, **141**, 70–78.
33 J. C. Gonçalves, A. F. P. Ferreira and A. E. Rodrigues, *Chem. Eng. Technol.*, 2019, **42**, 1169–1173.
34 N. Hosono and T. Uemura, *Acc. Chem. Res.*, 2021, **54**, 3593–3603.
35 N. Alsharif, B. Eshaghi, B. M. Reinhard and K. A. Brown, *Nano Lett.*, 2020, **20**, 7536–7542.

